Korean J. Chem. Eng., 39(7), 1709-1716 (2022)
DOI: 10.1007/s11814-022-1134-z

pISSN: 0256-1115
eISSN: 1975-7220

Multi-objective optimization of a methanol synthesis process: CO_2 emission vs. economics

Jae Hun Jeong*, Seungwoo Kim*, Myung-June Park,***,†, and Won Bo Lee*,†**

*School of Chemical and Biological Engineering, Seoul National University, Seoul 08826, Korea
**Department of Chemical Engineering, Ajou University, Suwon 16499, Korea
***Department of Energy Systems Research, Ajou University, Suwon 16499, Korea
(*Received 30 November 2021 • Revised 7 March 2022 • Accepted 2 April 2022*)

Abstract−This work addresses the modeling and multi-objective optimization of methanol synthesis to efficiently utilize CO_2 from the CO_2 emissions and economics perspectives. Kinetic reactors for reforming and methanol synthesis reactions were used in the process simulator for modeling the entire process, and multi-objective optimization was conducted using the developed process model to maximize CO_2 reduction and the economic profit. The feed composition, operating temperature and pressure of the reformer, and utility temperature of the methanol synthesis reactor were considered as arguments in the non-dominated sorting genetic algorithm (NSGA II) method with the net change of CO_2 and economic profit as the objective elements, and the Pareto front showed a trade-off between CO_2 reduction and economic profit. When the amount of CH_4 in the feed was fixed at 500 kmol/h, CO_2 reduction was 11,588 kg/h, whereas the profit was −5.79 million dollars per year. Meanwhile, a maximum profit of 20 million dollars per year resulted in CO_2 emissions of 7,201 kg/h. The feed composition had the most significant influence on both objective elements (net change of CO_2 and economics); as CO_2 in the feed increased, CO_2 reduction increased and profit decreased, while the increase of H_2O in the feed increased CO_2 emissions and profit.

Keywords: Methanol Synthesis Process, Reforming, Multi-objective Optimization, Economic Analysis, CO_2 Reduction

INTRODUCTION

Since the Industrial Revolution, the increase in greenhouse gas concentrations has resulted in severe global warming. As many climate change abnormalities have already occurred, several countries insist on a net CO_2-zero policy, and research on carbon capture and storage (CCS) and carbon capture and utilization (CCU) has been actively conducted. Various CCS and CCU methods include post-combustion, direct air capture, and biological capture, while polycarbonation, mineralization, biological utilization, photosynthesis, electrolysis, and enhanced oil recovery are some of the methods of CO_2 utilization [1]. CO_2 can be converted to different substances and used as feedstock in many reactions, including 123 reactions reported in the literature [2]. Some of the CO_2 utilization reactions, such as reforming, the synthesis of methanol (MeOH), dimethyl ether (DME), dimethyl carbonate (DMC) [3], formic acid [4], and urea [5], have been described in detail.

Among the many methods of CO_2 utilization, MeOH synthesis has been studied extensively because of its fuel quality and high demand. Because H_2 is essential for converting CO_2 into MeOH, many reaction routes, such as steam reforming, partial oxidation (POX), auto thermal reforming (ATR), water-gas-shift (WGS), and other catalytic reactions, have been introduced to produce H_2. In addition, photoelectrochemical processes and electrolysis using renewable energy have also been developed [6,7]. Dry (CO_2) reforming of CH_4 was adopted as an appropriate method because it can utilize CO_2 while producing hydrogen. The kinetics of mixed reforming of CH_4, composed of steam and dry reforming, and WGS, have been developed to analyze the effects of GHSV (gas hourly space velocity) and pressure on reforming [8]. It is difficult to utilize CO_2 because it is a very stable molecule, and many types of catalysts and mechanisms have been studied to convert CO_2 into MeOH. For MeOH synthesis, several reaction kinetics related to CO and CO_2 hydrogenation have been developed. Kinetics of CO and CO_2 hydrogenation and WGS over Cu-Zn-Al catalysts were developed under 15-50 bar and 210-245 °C [9]. The design of a large-scale MeOH synthesis process was proposed using the kinetics of reforming and MeOH synthesis, and the process model was used to evaluate the effects of reaction temperature, CO_2 fraction in the feed, and the recycling route on MeOH productivity, and CO and CO_2 conversion [10]. In addition, techno-economic analysis of the MeOH synthesis process with mixed reforming showed that the CO_2-utilized gas-to-MeOH process (CGTM) can be economically feasible in the plant scale range of 2,500-5,000 tons per day [11].

Many efforts have been made to analyze and improve the MeOH synthesis process. Multi-objective optimization of steam reforming was conducted by dynamic simulation and genetic algorithms, with the maximization of CH_4 conversion and minimization of a stoichiometric parameter as the objectives. It was proved that the tran-

†To whom correspondence should be addressed.
E-mail: mjpark@ajou.ac.kr, wblee@snu.ac.kr

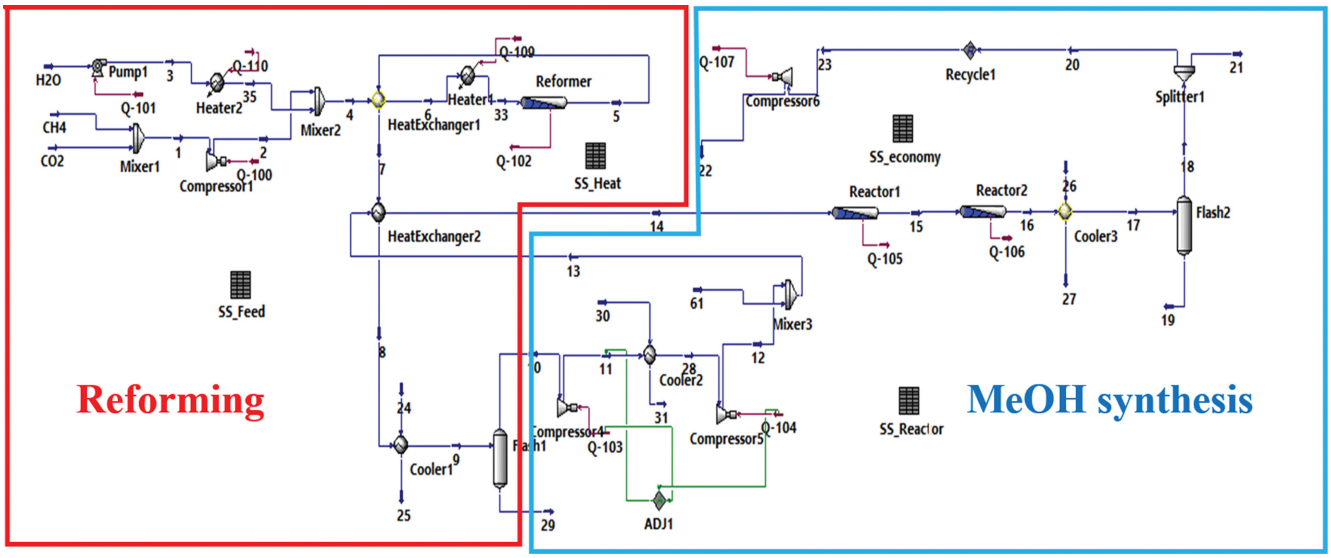

Fig. 1. Scheme of reforming and MeOH synthesis process.

sition period had the greatest effect on the objective function [12]. Using H_2 and CO_2, various MeOH production processes were studied; MeOH plant, electrolysis plant, fuel cost, etc.), and economic analysis was conducted under the situation where prices are fluctuating [13].

Previous studies related to the modeling of CO_2 utilization processes have mainly focused on the economy. However, as global warming has become increasingly severe, regulations on CO_2 emissions have been strengthened, and studies on CO_2 reduction have been conducted accordingly. The potential of CO_2 reduction, market scale, and thermodynamic characteristics of some reactions, including the production of MeOH, DME, DMC, formic acid, aldehydes, and urea have been described [7]. MeOH synthesis from CO_2 and green H_2 was studied, where two methods of MeOH production were introduced: one with direct CO_2 hydrogenation, and the other with reforming, followed by CO and CO_2 hydrogenation. Under the best conditions, 1.6 tons of CO_2 could be reduced per ton of MeOH [14].

Although CO_2 is consumed in the process streams, it can still be generated via energy consumption during the process. Therefore, it is necessary to study CO_2 utilization from the perspective of both CO_2 consumption by the reactions and CO_2 emissions from energy requirements, such as heating and compression. In this study, the MeOH synthesis process using CO_2, CH_4, and H_2O as feedstock was studied from the perspective of both CO_2 reduction and economy. Syngas was produced by reforming, and MeOH was produced by CO and CO_2 hydrogenation. After a process model for the entire process was developed by implementing kinetic reactor models in the simulator for both reforming and MeOH synthesis [8,10], a case study was conducted to understand the characteristics of the MeOH synthesis process. The process simulation was conducted using HYSYS (Aspen Technology). Because too many arguments require considerable computation load for case studies, the number of arguments was reduced by sensitivity analysis. Multi-object optimization (NSGA II) was conducted using Python and HYSYS spreadsheets to consider a trade-off between CO_2 reduction and economic profit, and the Pareto front was also identified.

METHOD

1. Reforming

The purpose of reforming is to produce syngas from CH_4, CO_2, and H_2O. The reforming process is shown in Fig. 1, where the reformer feed is a mixture of CH_4, CO_2, and H_2O. The feed conditions were fixed at 25 °C and 101 kPa, and it was assumed that the CO_2 supplied was 100% pure. Compressors and heaters were installed before the reformer because it was operated at 500-1,200 kPa and 750-900 °C. For thermodynamics, the Peng-Robinson equation was chosen, and the tube number, length, and diameter were specified at 80, 10 m, and 0.1016 m, respectively, resulting in a total volume of 12.972 m^3. Note that the size of the single tube that was determined in our previous work [10] was used without modification, while the number of tubes was adjusted by 1.6 times so that the residence time was maintained. Because the reforming reaction rate is very fast, the early part of the tube was in a kinetic regime, and the temperature was abruptly decreased by the endothermic reaction. In the later part, it was in a thermodynamic regime, and the temperature increased owing to an excessive supply of heat to the reformer. Water in the reformer effluent was evacuated in a flash vessel (Flash1 in Fig. 1) to prevent it from entering the MeOH synthesis reactor. The overall reactions and rate equations of the present study are as follows, and the kinetic parameters were used without modification [8,10]:

SRM1 (steam reforming of methane): $CH_4+H_2O \Leftrightarrow CO+3H_2$ (1)

SRM2 (steam reforming of methane): $CH_4+2H_2O \Leftrightarrow CO_2+4H_2$ (2)

WGS (water-gas shift): $CO+H_2O \Leftrightarrow CO_2+H_2$ (3)

DRM (dry reforming of methane): $CH_4+CO_2 \Leftrightarrow 2CO+2H_2$ (4)

$$r_{SRM1}=\frac{k_{SRM1}\left(f_{CH_4}f_{H_2O}-\frac{f_{H_2}^3 f_{CO}}{K_{pSRM1}}\right)/f_{H_2}^{2.5}}{\left[1+K_{CO}f_{CO}+K_{H_2}f_{H_2}+K_{CH_4}f_{CH_4}+K_{H_2O}\left(\frac{f_{H_2O}}{f_{H_2}}\right)\right]^2} \quad (5)$$

$$r_{SRM2}=\frac{k_{SRM2}\left(f_{CH_4}f_{H_2O}^2-\frac{f_{H_2}^4 f_{CO_2}}{K_{pSRM2}}\right)/f_{H_2}^{3.5}}{\left[1+K_{CO}f_{CO}+K_{H_2}f_{H_2}+K_{CH_4}f_{CH_4}+K_{H_2O}\left(\frac{f_{H_2O}}{f_{H_2}}\right)\right]^2} \quad (6)$$

$$r_{WGS}=\frac{k_{WGS}\left(f_{CO}f_{H_2O}-\frac{f_{H_2}f_{CO_2}}{K_{pWGS}}\right)/f_{H_2}}{\left[1+K_{CO}f_{CO}+K_{H_2}f_{H_2}+K_{CH_4}f_{CH_4}+K_{H_2O}\left(\frac{f_{H_2O}}{f_{H_2}}\right)\right]^2} \quad (7)$$

$$r_{DRM}=\frac{k_{DRM}\left(f_{CH_4}f_{CO_2}-\frac{f_{H_2}^2 f_{CO}^2}{K_{pDRM}}\right)}{[(1+K_{CH_4}f_{CH_4}+K_{CO}f_{CO})(1+K_{CO_2}f_{CO_2})]} \quad (8)$$

2. MeOH Synthesis Reactor

The MeOH synthesis reactor was used to produce MeOH from syngas. Fig. 1 displays the MeOH synthesis, which consisted of two reactors. MeOH synthesis occurred at 5,000 kPa, and the wall temperature was set at 180-230 °C. The inlet stream of the MeOH synthesis reactor was compressed using two compressors to boost energy efficiency. In our previous work [10], an inert material was used in the early part of the reactor to prevent an abrupt increase in temperature. To consider this feature, two reactors were employed in the process model, with the first reactor containing 50% inert material and the second reactor containing only catalysts; the kinetic parameters changed with the inert percentage. The two MeOH synthesis reactors had a tube diameter of 0.0411 m, tube number of 7200, and lengths of 4.4 m (the first reactor) and 8.46 m (the second reactor). The size of the single tube in the methanol synthesis reactor was specified to be the same as that of our previous work [10]. Meanwhile, the amount of syngas from the reformer was increased compared to that of our previous work and there was a recycle stream for the reactor in this work, resulting in a higher flow rate at the reactor inlet by 5-10 times than our previous work. Therefore, the number of tubes of the methanol synthesis reactor was increased for the residence time to be maintained [8,10]. The amount of CH_4 in the feed was set at 500 kmol/h for commercial scale (methanol production of 100 TPD). The MeOH synthesized in the MeOH reactor effluent was separated at the bottom of a flash vessel (Flash2 in Fig. 1) at 25 °C. The recovered gas in the flash vessel was recycled to the inlet of the MeOH synthesis reactor with a purge stream to prevent the accumulation of inert gases. The overall reactions and rate equations of MeOH synthesis were as follows, and kinetic parameters were used without modification [10]:

CO hydrogenation: $CO+2H_2 \Leftrightarrow CH_3OH$ (9)

CO_2 hydrogenation: $CO_2+3H_2 \Leftrightarrow CH_3OH+H_2O$ (10)

Reverse water-gas shift: $CO_2+H_2 \Leftrightarrow CO+H_2O$ (11)

DME production: $2CH_3OH \Leftrightarrow CH_3OCH_3+H_2O$ (12)

$$r_{CO}=\frac{k_A K_{CO}\left(f_{CO}f_{H_2}^{1.5}-\frac{f_{CH_3OH}}{K_{P,A}f_{H_2}^{0.5}}\right)}{(1+K_{CO}f_{CO})(1+K_{H_2}^{0.5}f_{H_2}^{0.5}+K_{H_2O}f_{H_2O})} \quad (13)$$

$$r_{CO_2}=\frac{k_C K_{CO_2}\left(f_{CO_2}f_{H_2}^{1.5}-\frac{f_{H_2O}f_{CH_3OH}}{K_{P,C}f_{H_2}^{0.5}}\right)}{(1+K_{CO_2}f_{CO_2})(1+K_{H_2}^{0.5}f_{H_2}^{0.5}+K_{H_2O}f_{H_2O})} \quad (14)$$

$$r_{RWGS}=-\frac{k_B K_{CO_2}\left(f_{CO_2}f_{H_2}-\frac{f_{CO}f_{H_2O}}{K_{P,B}}\right)}{(1+K_{CO_2}f_{CO_2})(1+K_{H_2}^{0.5}f_{H_2}^{0.5}+K_{H_2O}f_{H_2O})} \quad (15)$$

Table 1. Equipment purchased cost, and utility and feed price [16,19,22] (The value of the M&S index in 1968 is 280, while that in 2018 is 1638.2)

Equipment		Purchased cost	
Reactor		$(M\&S/280)\times 101.3\times(A)^{0.65}\times F_m\times F_c$	
Pump		$(M\&S/280)\times 517.5\times(bhp)^{0.82}\times F_c$	
Pressure - vessels, columns		$(M\&S/280)\times 101.9\times(D)^{1.066}\times H^{0.082}\times F_c$	
Tray		$(M\&S/280)\times 4.7\times(D)^{1.55}\times H\times F_c$	
Compressor		$(M\&S/280)\times 517.5\times(bhp)^{0.82}\times F_c$	
Heat exchanger		$(M\&S/280)\times 101.3\times(A)^{0.65}\times F_c$	
Furnace		$(M\&S/280)\times 5070\times(Q)^{0.85}\times F_c$	
		Value	Unit
Utility	Cooling water	0.013583	\$/ton
	Electricity	0.0727	\$/KWh
	Furnace fuel	$4.22*10^{-6}$	\$/kJ
Feed	CH_4	0.1267	\$/kg
	H_2O	0.000349	\$/kg
	CO_2	0	\$/kg
Product	MeOH	0.36	\$/kg

Table 2. Ratio factors used in the calculation of TCI [20]

Item	Ratio factors	Values
Direct cost	Purchase equipment	1.00
	Purchase equipment installation	0.47
	Buildings	0.8
	Yard improvements	0.1
	Service facility	0.7
	Instrumentation & controls	0.36
	Piping	0.68
	Electrical systems	0.11
Indirect cost	Engineering and supervision	0.33
	Contractor's fee	0.22
	Contingency	0.44
	Construction expenses	0.41
	Legal expenses	0.04
	Working capital	0.89

$$r_{DME}=\frac{k_{DME}K_{CH_3OH}^2\left(C_{CH_3OH}^2-\frac{C_{H_2O}C_{DME}}{K_{P,\,DME}}\right)}{\left(1+2\sqrt{K_{CH_3OH}C_{CH_3OH}}+K_{H_2O,\,DME}C_{H_2O}\right)^4} \quad (16)$$

3. Cost Estimation Method

The economy of the process was estimated using the profit and total production cost (TPC). TPC consists of a few factors listed in Table 3, total capital investment (TCI) and utility cost. The correlations for the equipment cost and the costs of utility, feed, and product are provided in Table 1 [15-21].

The following equation was used to calculate the total capital investment (TCI), and the ratio factors are listed in Table 2:

$$TCI=I_E\times\left(1+\sum_{i=1}^{n}RF_i\right) \quad (17)$$

where I_E and RF represent the total equipment cost and the ratio of the total equipment cost, respectively.

The TPC was calculated as follows:

$$TPC=(Utility+Operating\ \&\ Maintenance+Others)\times(100/90) \quad (18)$$

The correlations for operating/maintenance and other factors are shown in Table 3. Based on the TCI and TPC, the following equation was used to calculate the profit:

Table 4. Correlations for CO_2 equivalent

Item	CO_2 equivalent [kg/kJ]
Electricity	1.158×10^{-4}
Furnace fuel	7.06×10^{-5}

$$Profit=(Product\ revenue-TPC) \quad (19)$$

4. Calculation Method for CO_2 Equivalent

The utility and energy used in the process were converted to CO_2 equivalent using the correlations in Table 4 [22,23]. The efficiency of the furnace was assumed to be 70%.

The net change of CO_2 was calculated as follows:

$$\begin{aligned}\text{Net change of } CO_2=&(CO_2 \text{ equivalent by fuel usage})\\&+(CO_2 \text{ equivalent by electricity usage})\\&+(CO_2 \text{ in the process outlet streams}\\&-CO_2 \text{ in the process inlet streams})\end{aligned} \quad (20)$$

where positive net change corresponds to the emission of CO_2 (either the amount of CO_2 equivalent by energy usage was larger than the consumption of CO_2 by the reaction, or CO_2 was produced by the reaction) while a negative value represents CO_2 reduction.

5. Multi-objective Optimization

The non-dominated sorting genetic algorithm (NSGA II) method, which includes non-dominated sorting and crowding distance sorting to help find the Pareto front, was used because the relationship between the result and each variable is approximately linear. The non-dominated sorting algorithm makes elements close to the Pareto front, and the crowding distance sorting algorithm spreads the elements of the group far to find a wide Pareto front. The algorithm is shown in Fig. 2 and detailed algorithms can be found in [24,25].

The feed composition, reformer temperature, reformer pressure, and MeOH synthesis reactor wall temperature were considered as variables. The objective functions were defined with the net change of CO_2 and economic profit, whose calculation procedures are provided in Sections 2.3 and 2.4. To maintain the MeOH production rate, the amount of CH_4 in the feed was fixed at 500 kmol/h. At this amount of CH_4, if the amount of H_2O+CO_2 in the feed was lower than 400 kmol/h, a bad result at both objective functions was observed; thus, the lower bound of 400 kmol/h was specified for the amount of H_2O+CO_2.

Table 3. Correlation used in the calculation of TPC [18]

	Item	Assumptions & correlations
Operating & maintenance	Operating labor (OL)	60,000 $/labor/year, 4 labor/shift, 3 shift/day [Republic of Korea]
	Supervisory & clerical labor (S&C)	OL×0.2
	Maintenance & repairs (M&R)	FCI×0.06
	Operating supplies	M&R×0.15
	Laboratory charges	OL×0.15
Others	Depreciation	(TCI−0.05×TCI)/20 (5% salvage value, 20 year)
	Local taxes & insurance	FCI×0.02
	Plant overhead costs	(OL+S&C+M&R)×0.6
	Administration	(OL+S&C+M&R)×0.2

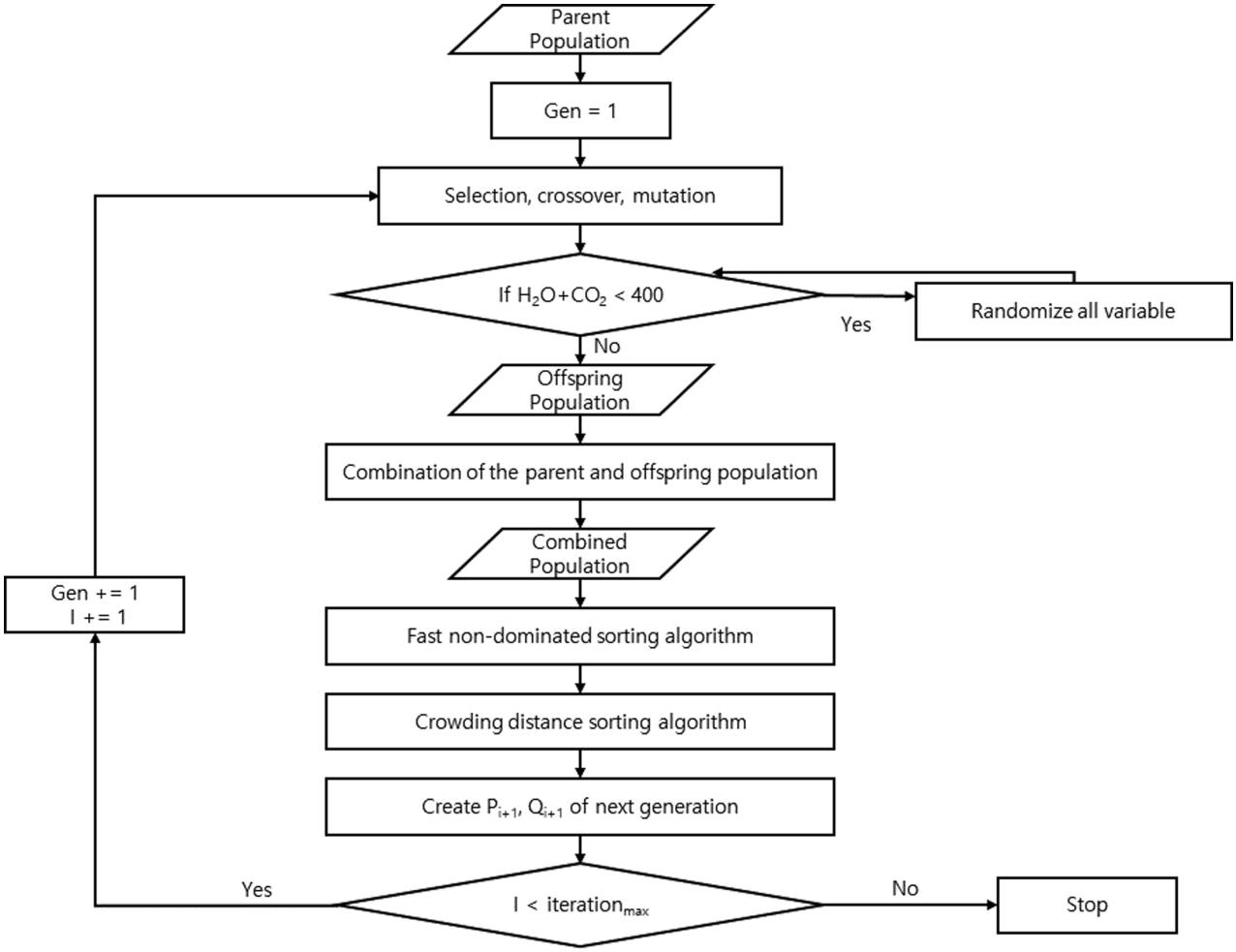

Fig. 2. Flow diagram of multi-objective optimization (NSGA II).

Process simulation was performed using HYSYS (Aspen Technology), and multi-objective optimization was performed using Python. The connection between HYSYS and Python was made using win32 dispatch [26], and the multi-objective optimization (NSGA II) was run using PYMOO [27] in a Python environment.

RESULTS AND DISCUSSION

1. Case Study: Effects of the Purge Ratio

Under the base conditions (feed CO_2=250 kmol/h, feed H_2O= 500 kmol/h, reformer pressure=500 kPa, reformer temperature= 800 °C, MeOH synthesis reactor wall temperature=200 °C), the purge ratio was varied, and the results are shown in Fig. 3. As the purge ratio decreased to 0.1, the profit increased owing to the increase in the MeOH production rate, and CO_2 emission was reduced (CO_2 reduction was increased), indicating that a small purge ratio is preferred for both profit and CO_2 reduction under the base condition; however, there were no negative values for the net change of CO_2 (always CO_2 emissions) for all the purge ratios. When the purge ratio was between 0 and 0.1, the profit and net change of CO_2 fluctuated, probably owing to the convergence issue with the overall mass balance. Therefore, the purge ratio was fixed at 0.1.

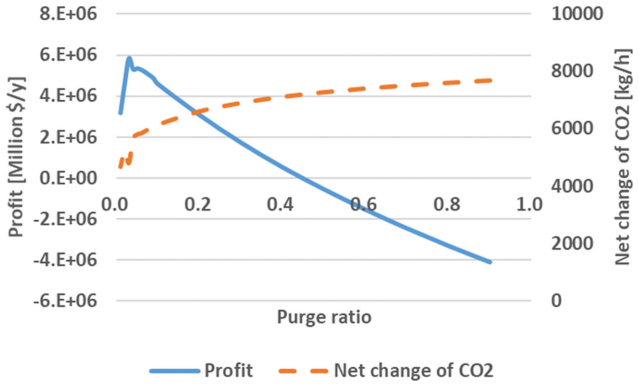

Fig. 3. Profit and net change of CO_2 as a function of purge ratio under the base condition.

2. Multi-objective Optimization

The amount of H_2O and CO_2 in the feed, reformer operating temperature and pressure, and MeOH synthesis reactor utility temperature were considered as the arguments in the optimization (the amount of CH_4 in the feed was 500 kmol/h). Fig. 4 shows the result of multi-objective optimization (population size: 80, offspring:

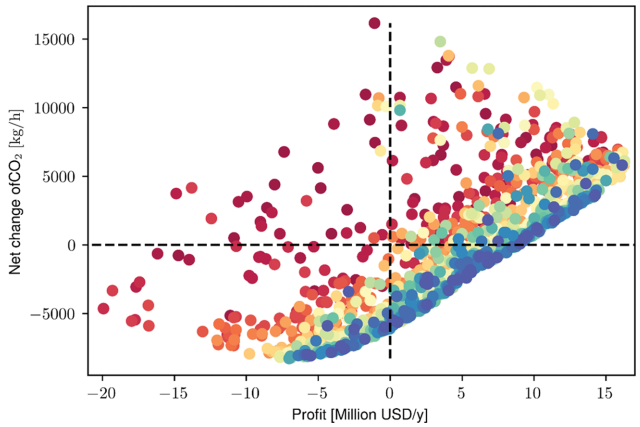

Fig. 4. Multi-objective optimization results when population size, offspring, generation, and the total number of data are specified at 80, 40, 40, and 1640, respectively. The arguments are the amount of H_2O and CO_2 in feed, reformer operating temperature and pressure, and MeOH synthesis reactor utility temperature. The first generation is marked with red dots, and the colors change from red to blue as the generation progresses (blue dots represent the last generation).

40, generation: 40, the total number of data: 1640).

Table S1 in the supplementary shows the last generation data in ascending order of profit. In all data, the reformer temperature and utility temperature of the MeOH synthesis reactor were close to 900 °C and 200 °C, respectively, and the operating pressure of the reformer ranged mostly between 600 and 700 kPa. This means that the temperatures and pressures of the reactors insignificantly influence the profit and net change of CO_2. Meanwhile, it can be seen that as CO_2 decreased and H_2O increased in the feed, both the profit and CO_2 emissions increased, indicating a trade-off between profit and CO_2 reduction.

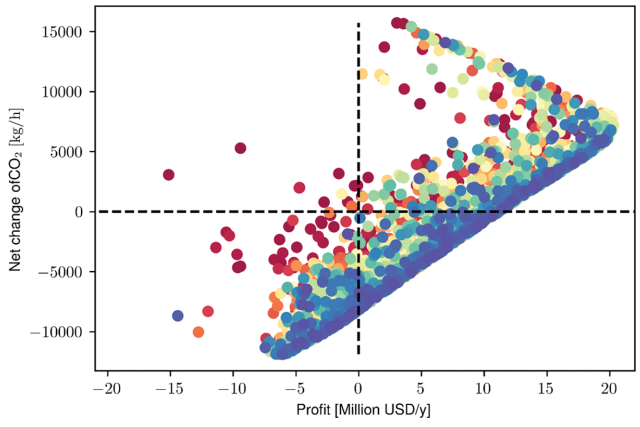

Fig. 5. Multi-objective optimization results when population size, offspring, generation, and the total number of data are specified at 80, 40, 100, and 4040, respectively. The arguments are the amount of H_2O and CO_2 in feed, reformer operating pressure, and MeOH synthesis reactor utility temperature. The first generation is marked with red dots, and the colors change from red to blue as the generation progresses (blue dots represent the last generation).

To identify a more accurate Pareto front, additional multi-objective optimization was performed with the upper limit of the amount of CO_2 increased to 700 kmol/h, and the reformer temperature fixed at 900 °C. Fig. 5 shows the result of the multi-objective optimization when the CO_2 feed, H_2O feed, reformer pressure, and MeOH synthesis reactor utility temperature are specified as the arguments (population size=80, offspring size=40, generation=100, total 4040 data), and Table S2 shows the last 40 generations of data in ascending order for profit. Note that the number of generations was specified to be large enough for the iterations to be converged. As shown in Fig. S1 in the Supplementary Information, the iterations converged when the generation was 50 and, thus, the generation was specified as 100 to guarantee the Pareto front was converged.

Upon reducing the number of arguments and increasing the range of CO_2 in the feed, the operating pressure of the reformer in the second optimization converged to 1,000-1,100 kPa (Table S2), and a wider Pareto front was determined, as shown in Fig. 5. As observed in the first optimization, the amount of H_2O and CO_2 in the feed played the most important role in the second optimization, and there was still a trade-off between profit and CO_2 reduction. Fig. 6 shows the relationship between the amount of H_2O and CO_2 in the feed with profit and net change of CO_2, where it is shown that high profit requires a high H_2O input (higher contribution of steam reforming than that of dry reforming), whereas low CO_2 emission or CO_2 reduction is accomplished at a high CO_2 input (higher contribution of dry reforming than that of steam reforming). This feature is attributable to the competition between steam and dry reforming when steam is added; thus, CO_2 consumption is decreased. However, the amount of hydrogen pro-

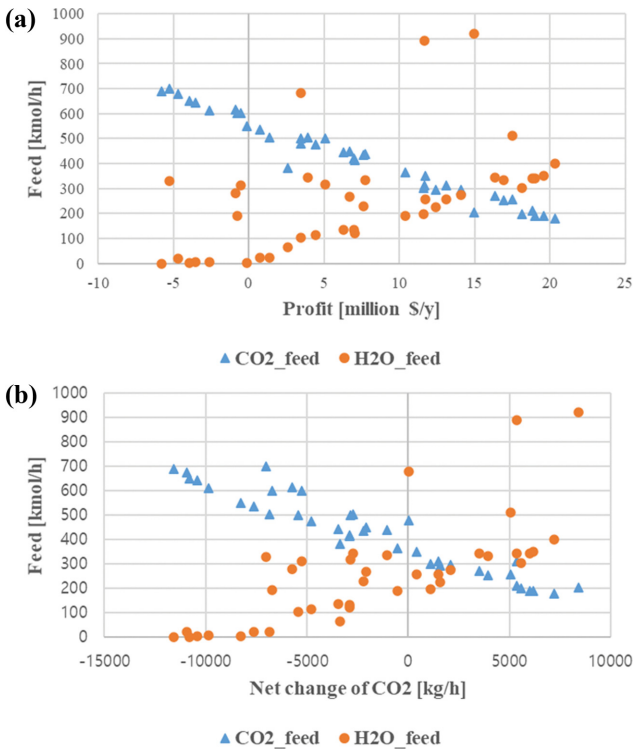

Fig. 6. The relationship of the amount of CO_2 and H_2O in the feed with (a) profit and (b) net change of CO_2.

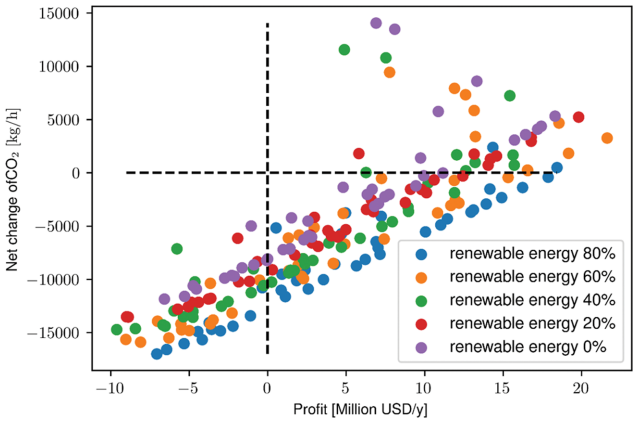

Fig. 7. Pareto front as a function of the use of renewable energy when population size, offspring, generation, and the total number of data are specified at 50, 40, 60, and 2410, respectively.

duced by steam reforming is larger than that by dry reforming (cf. Eqs. (1) and (4)); thus, a large amount of H_2O increases the MeOH production, increasing the profit of the process.

It is worth noting that the net change of CO_2 was estimated by considering the change in its amount in the stream and energy usage, with the assumption that the CO_2 feed was 100% pure. Therefore, actual CO_2 emission or reduction might be different for the actual plant. In addition, the shape of the Pareto front may vary when other conditions, such as the use of waste heat and the use of steam, are considered. However, despite the deviations from the actual values, an inverse relationship between CO_2 reduction and economic profit is expected in methanol synthesis processes.

Recently, the replacement of fossil fuel energy with renewable energy has been widely considered in many research works. Because the use of renewable energy influences CO_2 emission significantly, sensitivity analysis of the Pareto front was conducted for various fractions of renewable energy usage. The amount of CO_2 generated by electricity usage was adjusted proportionally to the degree of replacement by renewable energy; for example, CO_2 equivalent for 80% of renewable energy was reduced to 0.2 times of 100% use of fossil fuel energy. As shown in Fig. 7, CO_2 reduction was increased as more renewable energy was used. The use of renewable energy also influenced the profit. When the net change of CO_2 was zero, the profit for 80% use of renewable energy was increased approximately 1.75 times higher than that of 0% renewable energy.

CONCLUSIONS

Multi-object optimization (NSGA II) was applied to the MeOH synthesis process, and the resulting Pareto front showed that there was a trade-off between CO_2 reduction and economic profit. Despite the trade-off, there were conditions in which CO_2 reduction and economic profit were achieved simultaneously. At the maximum CO_2 reduction of 11,588 kg/h, the profit was −5.79 million dollars per year, while the maximum profit of 20 million dollars per year resulted in the maximum CO_2 emission (7,201 kg/h). Among the five variables (CO_2 and H_2O in the feed, reformer temperature and pressure, and utility temperature of the MeOH synthesis reactor), the amount of CO_2 and H_2O in the feed had the most significant influence on the objective elements. A large amount of CO_2 in the feed showed a large contribution of dry reforming, resulting in low CO_2 emission (high CO_2 reduction) at the expense of the economics of the process due to the small amount of hydrogen, that is, low MeOH production rate. Meanwhile, the increase in the amount of H_2O in the feed increased the economic profit as CO_2 emissions increased.

ACKNOWLEDGEMENT

This research was supported by the Technology Innovation Program (20015460) funded by the Ministry of Trade, Industry & Energy (MOTIE, South Korea).

SUPPORTING INFORMATION

Additional information as noted in the text. This information is available via the Internet at http://www.springer.com/chemistry/journal/11814.

REFERENCES

1. F. D. Meylan, V. Moreau and S. Erkman, *J. CO_2 Utilization*, **12**, 101 (2015).
2. A. Otto, T. Grube, S. Schiebahn and D. Stolten, *Energy Environ. Sci.*, **8**, 3283 (2015).
3. J. Ma, N. Sun, X. Zhang, N. Zhao, F. Xiao, W. Wei and Y. Sun, *Catal. Today*, **148**, 221 (2009).
4. T. Schaub and R. A. Paciello, *Angew. Chem. Int. Ed. Engl.*, **50**, 7278 (2011).
5. X. Xiang, L. Guo, X. Wu, X. Ma and Y. Xia, *Environ. Chem. Lett.*, **10**, 295 (2012).
6. P. Nikolaidis and A. Poullikkas, *Renew. Sust. Energy Rev.*, **67**, 597 (2017).
7. C.-H. Huang and C.-S. Tan, *Aerosol Air Quality Res.*, **14**, 480 (2014).
8. N. Park, M.-J. Park, S.-C. Baek, K.-S. Ha, Y.-J. Lee, G. Kwak, H.-G. Park and K.-W. Jun, *Fuel*, **115**, 357 (2014).
9. G. H. Graaf, E. J. Stamhuis and A. A. C. M. Beenackers, *Chem. Eng. Sci.*, **43**, 3185 (1988).
10. N. Park, M.-J. Park, K.-S. Ha, Y.-J. Lee and K.-W. Jun, *Fuel*, **129**, 163 (2014).
11. C. Zhang, K.-W. Jun, R. Gao, G. Kwak and H.-G. Park, *Fuel*, **190**, 303 (2017).
12. A. Alizadeh, N. Mostoufi and F. Jalali-Farahani, *Int. J. Chem. React. Eng.*, **5**, A19 (2007).
13. K. Atsonios, K. D. Panopoulos and E. Kakaras, *Int. J. Hydrogen Energy*, **41**, 2202 (2016).
14. É. S. Van-Dal and C. Bouallou, *J. Cleaner Production*, **57**, 38 (2013).
15. R. K. Sinnott, *Chemical engineering design*, Second edition. edn. Pergamon, Oxford (1993).
16. S. M. Walas, *Chemical process equipment: Selection and design*, Elsevier Science & Technology Books, Place of Publication Not Identified (1988).
17. Commodity Markets. https://www.worldbank.org/en/research/commodity-markets.

18. J. M. Douglas, *Conceptual design of chemical processes*, International edn. McGraw-Hill, New York, London (1988).
19. Home - Methanol Market Services Asia. https://www.methanol-msa.com.
20. M. S. Peters, *Plant design and economics for chemical engineers*, McGraw-Hill, New York (1958).
21. W. D. Seider, J. D. Seader and D. R. Lewin, *Product and process design principles: Synthesis, analysis and evaluation*, Rev. of: Process design principles, 1999, Wiley, New York (2004).
22. Homepage - U.S. Energy Information Administration (EIA). https://www.eia.gov.
23. CAMEO Chemicals | NOAA. https://cameochemicals.noaa.gov.
24. K. Deb, A. Pratap, S. Agarwal and T. Meyarivan, *Ieee T Evolut Comput*, **6**, 182 (2002).
25. C. Bao, L. Xu, E. D. Goodman and L. Cao, *J. Comput. Sci.*, **23**, 31 (2017).
26. GitHub - edgarsmdn/Aspen_HYSYS_Python: Aspen HYSYS - Python connection. https://github.com/edgarsmdn/Aspen_HYSYS_Python.
27. J. Blank and K. Deb, *IEEE Access*, **8**, 89497 (2020).

Supporting Information

Multi-objective optimization of a methanol synthesis process: CO_2 emission vs. economics

Jae Hun Jeong*, Seungwoo Kim*, Myung-June Park,***,†, and Won Bo Lee*,†**

*School of Chemical and Biological Engineering, Seoul National University, Seoul 08826, Korea
**Department of Chemical Engineering, Ajou University, Suwon 16499, Korea
***Department of Energy Systems Research, Ajou University, Suwon 16499, Korea
(*Received 30 November 2021 • Revised 7 March 2022 • Accepted 2 April 2022*)

Table S1. Dataset of the last generation in the first case of the multi-objective optimization (Fig. 4 in manuscript)

Arguments					Objectives	
Reformer temperature [°C]	MeOH synthesis reactor utility temperature [°C]	Reformer pressure [kPa]	CO_2 feed [kmol/h]	H_2O feed [kmol/h]	Profit [M$/y]	CO_2 emission [kg/h]
896.4	213.8	933.6	498.8	0.6	−5.8	−7,966.5
896.4	187.8	830	498.8	0.2	−5.5	−8,060.1
859.9	199.2	729.9	451.9	56.6	−4.4	−5,880.6
896.4	192.4	654	498.9	0.2	−4.1	−7,807.9
896.8	201.4	670.9	489.6	11	−3.5	−7,357.1
898.6	205.2	595.2	499.7	2.5	−3.2	−7,552.4
898.7	190.1	594.8	349.9	50.5	−2.9	−3,399.2
899.2	202	613.2	446.1	22.7	−2.5	−6,119.1
896.4	201.3	644.1	497.6	45.8	−1.8	−6,842.4
898.6	203.9	683.2	485.9	83.7	−0.4	−5,967.6
896.5	220	623.1	499.8	116.2	0.2	−5,481.8
898.4	194.9	616.6	486.5	102.2	0.5	−5,625.2
896.9	191.4	1,064.3	495.8	367.4	2.4	−2,754.3
896.4	198.9	640.6	498.1	202.4	2.6	−4,340.9
899	205.9	602.3	394.6	143.8	2.6	−2,341.4
898.6	198.5	595.7	468.1	211.5	2.6	−2,855.1
898.2	208.8	625.5	480.3	241.7	4.1	−3,294.1
898.6	202.4	786.5	491.9	342.2	4.3	−2,574.4
898.6	198.6	610.1	499.4	341.4	4.7	−2,517
899.2	207.9	634	435.3	236	5.3	−2,386.3
897.7	205.3	608.5	488.4	353.6	5.4	−2,081.7
898.6	203.6	607.8	491.1	384.5	5.6	−1,806.4
898.7	191.5	629.2	415.7	241	5.6	−1,985.2
898.5	209.1	637.5	485.2	465.8	6.2	−8,48.9
882.2	190.1	1,092.7	297.2	395.5	6.8	1,829.1
898.6	204.4	656.2	439	335	6.8	−1,312.6
893.9	191.5	701.6	413.6	339.7	6.8	−886
900	202	624.4	449.7	361.7	6.9	−1,212.6
899.7	202	625.1	435.8	361.6	7.4	−911.3
898.9	207.9	623.4	317.3	227.2	7.5	276.9
897.9	204.8	608.3	389.8	354.1	9.0	99.9
898.4	202	658.8	399	426.2	9.3	481.8
899.8	207	696	355.4	346.9	9.6	669.2
898.6	191.3	622.5	337.5	342.4	10.2	1,113.9
896.8	202.2	683.6	385	479.2	10.2	1,246.8
898.1	208.5	716.8	266.7	346.2	11.4	2,767.2
899.7	203.6	640.7	359.6	466.3	11.4	1,784
894.5	197.6	655.8	216.3	384.5	13.6	4,482.8
896.4	203.2	654.4	289.3	505	14.2	3,642
899.8	203.2	637	229.9	602	16.1	5,827.3

Table S2. Dataset of the last generation in the second multi-objective optimization (Fig. 5 in manuscript)

Arguments				Objectives	
MeOH synthesis reactor utility temperature [°C]	Reformer pressure [kPa]	CO_2 feed [kmol/h]	H_2O feed [kmol/h]	Profit [M$/y]	CO_2 emission [kg/h]
201.6	1,022.1	592.6	3.3	−1.6	−9,325.2
192.2	1,010.9	256.6	274.6	15.2	3,189.7
204.5	1,100.9	525.2	3.4	0.8	−7,360.7
201.3	1,080.8	378.4	187.4	9.9	−922.2
202.7	1,012.5	480.1	2.0	0.0	−6,723.8
196.2	1,057.2	317.0	329.4	14.0	2,225.4
193.1	1,013.0	455.0	141.2	5.6	−3,893.9
197.6	1,065.1	556.0	3.8	−0.2	−8,311.7
197.6	1,049.6	84.0	718.0	11.9	11,971.2
201.9	968.0	688.7	35.9	−4.9	−10,975.1
201.2	1,053.3	359.0	754.0	9.1	3,607.1
192.5	968.7	697.2	364.3	−4.1	−6,484.0
195.8	1,054.1	429.7	106.0	6.1	−3,564.3
209.4	1,032.6	609.3	8.1	−2.1	−9,569.9
198.1	1,007.3	635.6	2.9	−3.3	−10,377.7
200.2	1,029.9	316.7	314.0	14.0	2,010.6
200.1	1,054.0	484.7	108.3	4.2	−4,969.0
202.3	1,037.4	542.5	670.4	−0.9	−1,851.3
204.1	1,010.7	237.0	608.0	17.7	6,135.9
195.4	1,027.1	318.6	218.1	12.2	879.1
204.6	1,054.0	330.9	314.9	13.2	1,723.3
209.0	1,051.2	385.3	213.0	9.7	−856.8
192.9	1,054.1	352.5	234.9	11.4	230.6
197.6	1,025.6	677.1	127.1	−4.4	−9,383.1
203.9	986.4	394.9	141.2	7.1	−2,396.2
200.7	1,024.0	577.4	19.0	−0.8	−8,711.9
199.7	1,021.4	372.8	246.3	10.7	−299.2
206.4	1,018.3	699.5	259.2	−4.5	−7,757.6
199.6	1,059.2	512.5	2.6	0.8	−7,274.9
192.1	1,057.0	633.5	9.2	−3.6	−10,215.5
200.4	972.6	353.4	137.5	6.7	−1,539.0
197.8	1,023.0	416.1	136.1	7.1	−2,885.7
199.5	1,024.1	605.8	0.6	−2.1	−9,699.7
196.3	1,012.0	250.3	344.3	17.2	4,097.7
201.5	1,024.3	380.6	185.5	9.4	−1,223.8
204.7	1,054.6	663.2	4.2	−4.5	−10,906.3
201.9	1,030.7	43.0	876.0	6.9	14,072.2
209.6	1,032.6	612.9	8.4	−2.3	−9,640.7
206.3	1,053.1	508.4	74.9	2.8	−6,029.1
198.3	1,052.5	524.3	32.1	1.4	−7,122.7

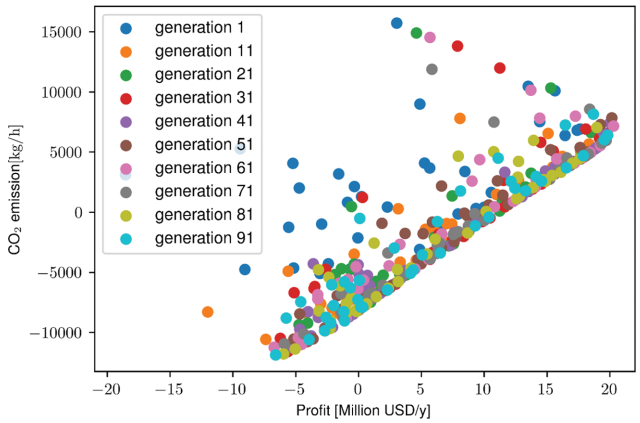

Fig. S1. Multi-objective optimization results for each generation; all the data are provided in Fig. 5.